HiSST: 3rd International Conference on
High-Speed Vehicle Science Technology
14 -19 April 2024, Busan, Korea

Numerical Investigation of Shock Induced Mixing Enhancement in Cavity-Based Scramjet Combustor

Tomoaki Nara[1], Chihiro Fujio[2], Hideaki Ogawa[3]

Abstract

Scramjet engines are promising propulsion systems for space transportation and long-range high-speed transportation. For efficient thrust generation in a scramjet, not only drag reduction but also high mixing efficiency is required. In this study, the characteristics of fuel mixing due to shock wave interactions in a combustor with transverse injection and cavity-based flameholding are investigated, with a focus on performance and flowfields. The performance and flowfields are evaluated in the presence of impingement oblique shock waves at various locations for a particular cavity geometry. Computational fluid dynamics simulations have been performed to calculate steady flowfields. As a result, it has been verified that the mixing efficiency is improved when the shock wave is incident on the cavity. It has also been found that the mixing efficiency is most improved when the shock wave interacts with the rear edge of the cavity. Further, the drag has also been found to be the lowest in the situation where the shock wave impinges on the rear end of the cavity.

Keywords: *scramjet engine, cavity-based flameholder, mixing enhancement, shock wave interaction*

1. Introduction

Supersonic combustion ramjet (scramjet) engines hold great promise for applications in accessing low Earth orbit and enabling long-range high-speed air transportation. As air-breathing engines, they eliminate the need for onboard oxidizers and can achieve high specific impulse [1,2]. Additionally, due to the absence of rotating parts, these engines are expected to have a simple structure and high reliability. Numerous studies have been conducted, and several flight experiments have been carried out toward the practical application of scramjet-powered flight vehicles [3,4].

However, the realization of a scramjet-powered flight vehicle has been hindered to date by various issues. One of the challenges has been efficient and stable combustion in the combustor. The residence time of supersonic air passing through the combustor is on the order of milliseconds, which means that fuel/air mixing, ignition, and combustion must occur within such an extremely short timeframe. Therefore, fuel must be mixed as quickly and uniform as possible. To enhance mixing in the combustor, various strategies have been investigated, such as struts, ramps, pylons, transverse injection, cavities, and shock-wave interaction [5-11].

Mai *et al*. investigated the interaction of impinging shock waves and transverse jet flow in mixing and combustion in supersonic airflows both experimentally and numerically [12]. As a result, it has been

[1] *Department of Aeronautics and Astronautics, Graduate School of Engineering, Kyushu University, 744 Motooka Nishi-ku, Fukuoka 819-0395, Japan, nara.tomoaki.455@s.kyushu-u.ac.jp*
[2] *Department of Aeronautics and Astronautics, Graduate School of Engineering, Kyushu University, 744 Motooka Nishi-ku, Fukuoka 819-0395, Japan, fujio.chihiro.354@s.kyushu-u.ac.jp*
[3] *Department of Aeronautics and Astronautics, Graduate School of Engineering, Kyushu University, 744 Motooka Nishi-ku, Fukuoka 819-0395, Japan, hideaki.ogawa@aero.kyushu-u.ac.jp*

confirmed that the introduction of impinging shock waves just below the injection slot creates circulation, which enhances mixing and extends the residence time in the recirculation zone. Schetz *et al*. investigated the effects of molecular weight and shock waves on transverse injection in supersonic flow and confirmed that mixing efficiency increases when shock waves impinge downstream of the injector, regardless of the molecular weight of the material being injected [13]. Such a shock-induced mixing enhancement strategy not only promotes mixing and flame holding but also has the advantage of incurring less drag than an in-stream device. On the other hand, these advantages also apply to cavities. Gruber *et al*. evaluated flowfields characteristics of various cavity geometries and confirmed that changes in the backward ramp angle affect shear and changes in the magnitude of drag, length of residence time, and flow stability [10]. Ukai *et al*. varied the position of lateral jets for rectangular open cavities and investigated mixing characteristics [14]. As a result, it has been confirmed that placing the injector near the front edge of the cavity resulted in higher mixing characteristics. However, it has been pointed out that this arrangement may cause the flow over the cavity to become unstable, resulting in the loss of flame stability characteristics, and measures such as ramping the back wall have been proposed. This study investigates the flowfields caused by the interaction of transverse injection with a trapezoidal cavity and oblique shock waves. It is believed that higher mixing can be achieved by combining these two techniques. The results are scrutinized to reveal the structure of the cavity flowfields with shock waves.

2. Methodologies

Configurations

The present study investigates the effects of the interaction between oblique shock waves and the free shear layer above the cavity in a scramjet engine. Figure 1 schematically shows the geometric configuration and design variables considered in the present study. The geometry consists of a ramp serving as a shock generator, a transverse wall injection slot, and a trapezoidal cavity. The ramp generates an incident shock wave that interacts with the recirculation region in the cavity, thereby varying the flowfields and mixing performance. To evaluate the effects of the shock interaction location on the mixing performance, the distance between the ramp and the injection slot is used as a variable.

The inflow condition considered in this present study is summarized in Table 1. The inflow boundary condition is obtained by calculating the profile of the developed turbulent boundary layer on a 150-mm duct based on the condition of Table 1. The injection condition is shown in Table 2. The injection condition is determined to maintain a fuel/air equivalent ratio of Φ = 0.375.

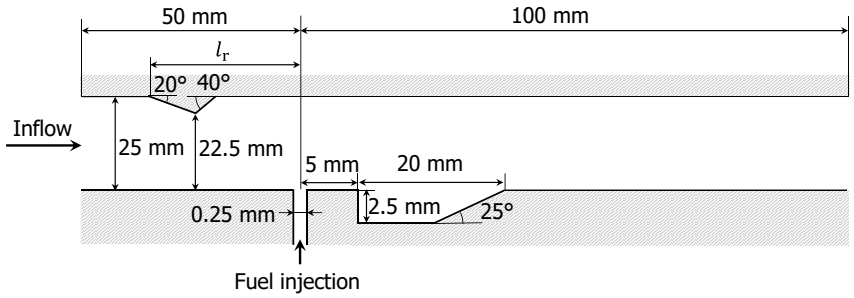

Fig 1. Schematic of two-dimensional combustor with design variables

Table 1. Inflow condition

Mach number	Static pressure	Static temperature	O_2 mole fraction	N_2 mole fraction
3.5	59,850 Pa	800 K	0.79	0.21

Table 2. Injection condition

Mach number	Static pressure	Static temperature	Fuel/air equivalent ratio
1	64,215 Pa	250 K	0.375

Test case

The present study investigates the effects of the oblique shock wave impingement location and cavity shape on mixing performance in a transverse slot injection cavity-based combustor in a parametric manner. The values of design variables for the cases considered are summarized in Table 3.

The location of oblique shock wave impingement is controlled by varying the distance between the ramp base and the injection slot, with three different locations. The case that interacts the most upstream of the three (case 1) is determined to have the shock wave incident near the front wall of the cavity.

The case that interacts most downstream (case 3) is determined to have the shock wave incident at the rear edge of the cavity (the end of the ramp). The middle case is determined at the centre of the above two cases.

Table 3. Test case for investigating the effect of location of shock impingement

Case name	l_r [m]
Case 1	0.034
Case 2	0.024
Case 3	0.014
No ramp	-

Characteristic parameters

The characteristics of shock wave interaction in cavity-based combustors are represented by three parameters: mixing efficiency, total pressure loss, and force in the streamwise direction.

When evaluating mixing performance, the degree of fuel diffusion and the ratio of air to fuel are important factors. In this present study, they are employed as the mixing efficiency. The mixing efficiency is the mass ratio of combustible fuel to supplied fuel and is defined as:

$$\eta_{\mathrm{m}} \equiv \frac{1}{\dot{m}_{\mathrm{H_2}}} \int \min\left(c_{\mathrm{H_2}}, \frac{c^{\mathrm{S}}_{\mathrm{H_2}}}{c^{\mathrm{S}}_{\mathrm{O_2}}} c_{\mathrm{O_2}}\right) \mathrm{d}\dot{m} \tag{1}$$

where the stoichiometric mass fractions of oxygen $c^S_{O_2}$ and hydrogen $c^S_{H_2}$ are 0.226 and 0.028, respectively.

In this study, the force in the streamwise direction on the combustor is evaluated in order to investigate drag and its causes. This force is calculated by integrating the momentum per unit area of the combustor inlet cross section minus an optional cross section. It is defined as:

$$F_x \equiv \int_0^{0.0025} (p + \rho u^2) dy \Big|_{x=-0.05} - \int_{y_{\min}}^{y_{\max}} (p + \rho u^2) dy \tag{2}$$

where x is the axis in the direction of inflow with the center of the injector as 0 and y is the axis in the direction of injection with the injector outlet as 0. Also, $y_{\min}$ and $y_{\max}$ are the y coordinates of the bottom and top walls, respectively, at a certain x section.

Computational fluid dynamics (CFD)

Flowfields in the cavity-based combustor are obtained by ANSYS Fluent 2023 R1[15]. The calculations are performed on a density basis, and the governing equations are Reynolds-averaged Navier-Stokes (RANS) equations. The two-equation shear stress transportation (SST) k-ω is employed for turbulence modeling. This turbulence model is selected due to its capability to resolve flowfields with large adverse pressure gradient as well as boundary layer separations accurately [9]. The inflow gas is assumed to be an ideal gas, and the top and bottom walls are adiabatic walls. The calculations are performed until the energy residuals reach 5e-4 for all cases.

The computational domain is constituted by the structural mesh generated by Gmsh[16]. Figure 2 shows the mesh for the baseline geometry with and without ramps. The mesh is progressively refined toward the walls to properly resolve the boundary layer and the cavity surface flowfields.

The number of computational cells is determined by a mesh sensitivity study. This study is conducted on three different resolution meshes, *i.e.*, a coarse mesh with 127,500 cells, a nominal mesh with 509,800 cells, and a fine mesh 2,038,800 cells. Figure 3 shows the distributions of wall pressure and shear stress so as to visualize the effect of mesh resolution. It has been found that the results with nominal and fine meshes agree reasonably well. Figure 4 compares the mixing efficiency for the three cases. To estimate the exact values of the performance parameters, Richardson extrapolation has been employed, and results from three different meshes are substituted [17]. As a result, it is confirmed that the fine mesh takes values that are close and similar to the extrapolated values. In this study, the nominal mesh is employed, as it balances the computational cost and the accuracy of the performance calculations.

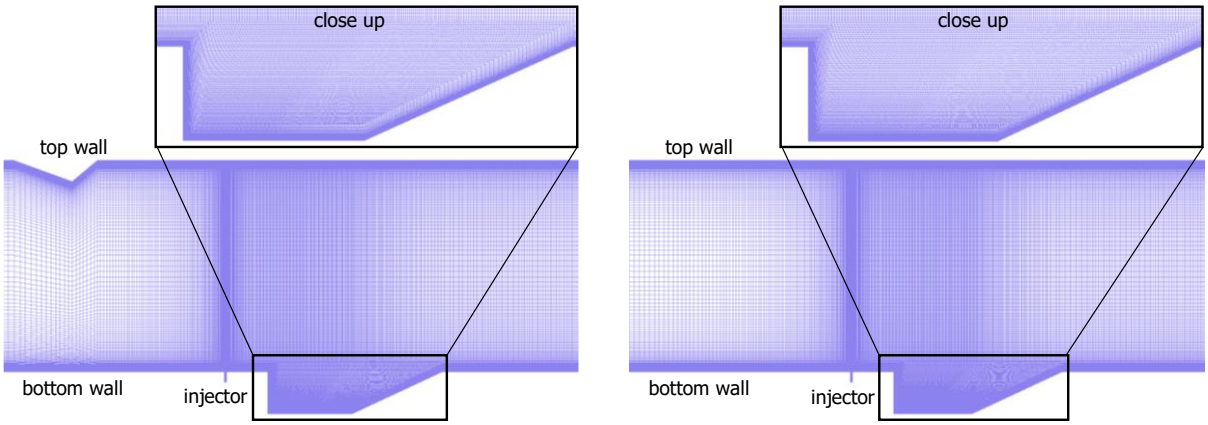

(a) without ramp (b) with ramp

Fig 2. Mesh configuration and boundary conditions

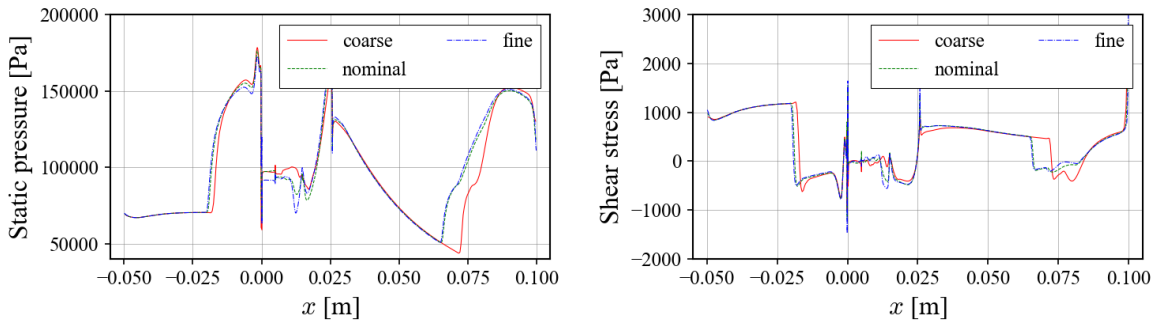

(a) Static pressure (b) Wall shear stress

Fig 3. Distributions of wall static pressure and shear stress for different mesh resolusions

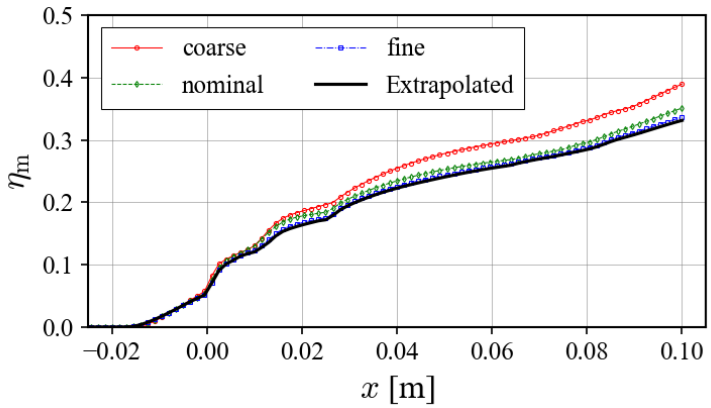

Fig 4. Comparison of mixing efficiency for different mesh resolutions

3. Results

Effects of shock interaction location

In this section, the results of CFD simulations for different locations of oblique shock impingement are discussed in terms of their effects on the flowfields and mixing performance. To illustrate the structure of the flowfields, Fig. 5 shows the Mach number distribution for Case 1. An oblique shock wave is formed from the top wall by the ramp. This shock wave is incident on the cavity. Also, a separation shock wave is induced upstream of the fuel injection. In the cavity, a subsonic recirculation region is formed, and an oblique shock wave stands at the rear edge of it. In this study, this shock wave is called a "*cavity shock*".

Figure 6 shows the relationship between the location of the shock wave and the mixing efficiency. According to Fig. 6, the case with the shock wave incident most forward (Case 1) maintains a high mixing efficiency from the upstream of injection to the rear edge of the cavity (x = 0.025 m). However, downstream of the rear edge, the mixing efficiency of the case with the shock wave incident most backward (Case 3) increases at a high rate and exceeds the other cases with x = 0.04 – 0.05 m. These differences in trends lead to a discussion of the two separate cases upstream and downstream of the trailing edge of the cavity (x = 0.025 m).

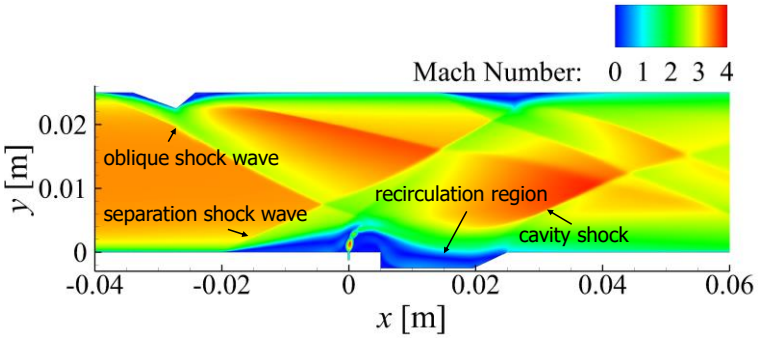

Fig 5. Mach number distribution for Case 1

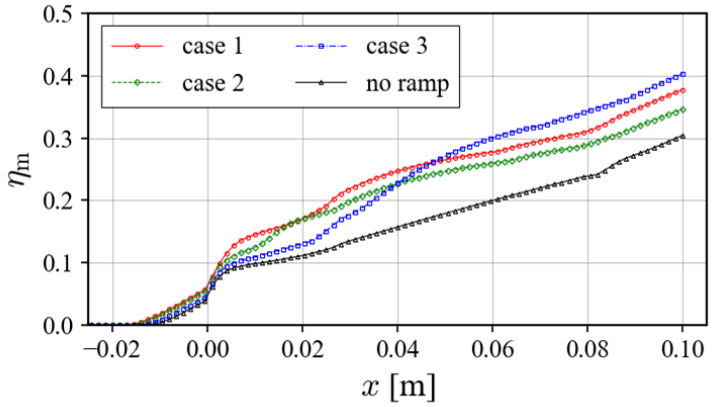

Fig 6. Comparison of mixing efficiency with shock impingment location

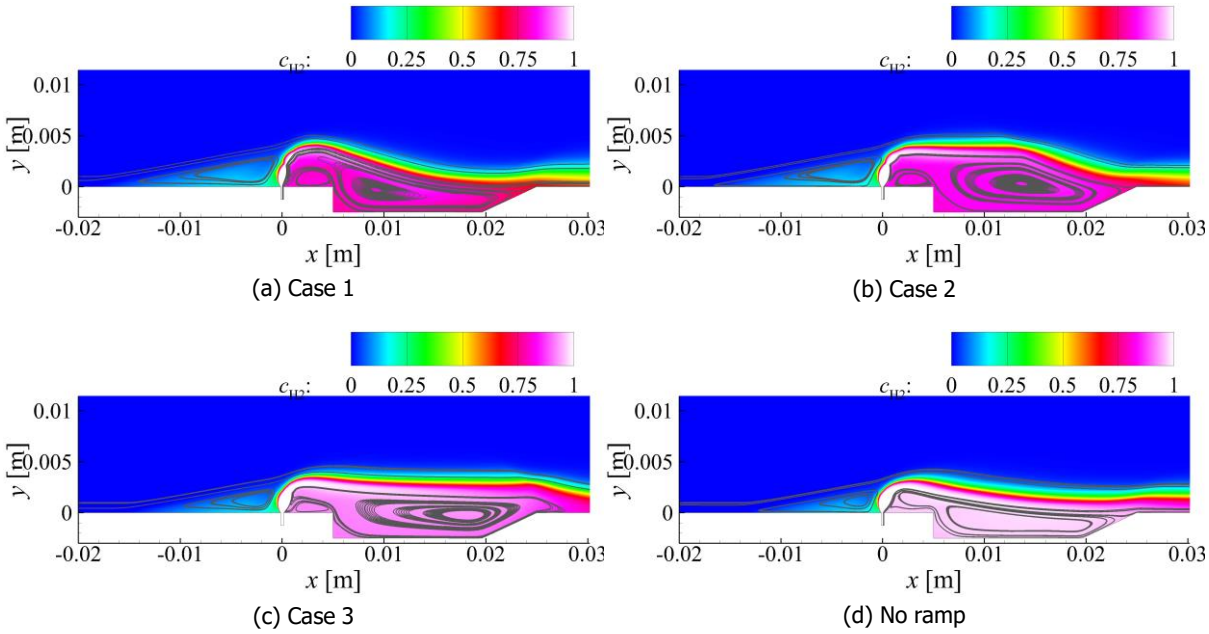

(a) Case 1 (b) Case 2

(c) Case 3 (d) No ramp

Fig 7. Hydrogen mass fraction distributions and streamlines

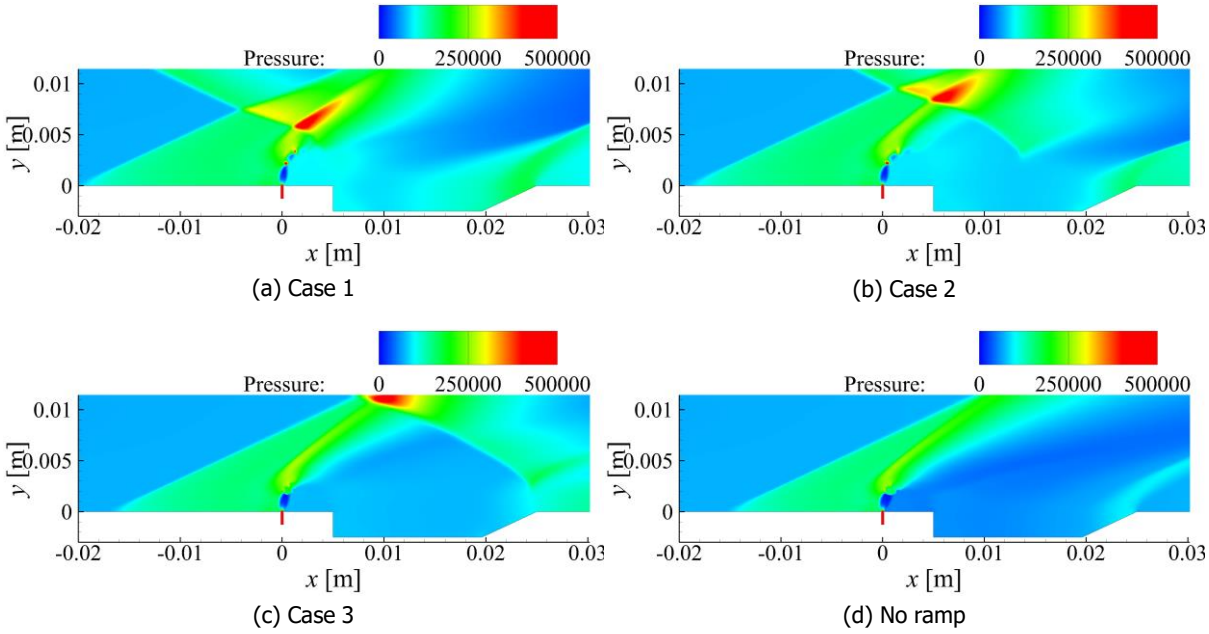

(a) Case 1 (b) Case 2

(c) Case 3 (d) No ramp

Fig 8. Static pressure distributions

Figure 7 shows the distributions and streamlines of the fuel mass fraction around the injector and the cavity to consider the mixing efficiency on the upstream side. The color map shows the mass fraction of hydrogen, and the gray line shows the streamlines around the cavity. In Fig. 7, around the injector, it is observed that the fuel injection penetration is higher, and the fuel mass fraction in the cavity is relatively small when the shock wave impinges on the upstream side. Additionally, at the upstream of the injector, the higher fuel penetration leads to a larger recirculation region. This suggests that the mixing efficiency upstream, especially upstream of the injector, is affected by the change in the height of the fuel penetration due to shock wave interaction. Also, the mixing efficiency upstream, especially in the cavity, is considered to be affected by the decrease in the hydrogen mass fraction due to the shock wave interaction.

To assessed shock wave interference and the height of penetration, Fig. 8 shows the static pressure distributions. In Fig. 8, around the downstream of the injector (x = 0 - 0.05 m), it shows that the

injector back pressure increases as the shock wave impinges upstream. This is due to the pressure increase caused by the cavity shock generated at the rear ramp of the cavity, which propagates into the cavity through the subsonic region. Since the main flow is diverted downward by the shock wave, the cavity shock at the back ramp tends to be stronger as a result of shock wave interaction, as shown in Fig. 8. Therefore, injector back pressure increases, and fuel penetration is increased. Furthermore, as the penetration increases, the separation shock wave upstream of the injector moves forward, and the recirculation area increases, as seen in Fig. 8. This explains the mixing efficiency upstream of the injector ($x \geq 0$ m) observed in Fig. 6.

Next, the fuel mass fraction in the cavity and shock wave interaction are examined. The varying magenta-colored regions within the cavity in Fig. 7 indicate a decrease in hydrogen mass fraction as shock waves interact upstream. The hydrogen mass fraction decreases from 1, which means that the fuel is mixed with air, contributing to an increase in mixing efficiency. To consider the fuel mass fraction and shock wave interaction, the distributions of the high hydrogen mass fraction region are shown in Fig. 9. Regions with a mass fraction of 0.95 or higher are displayed in color, and regions with a mass fraction of less than 0.95 are displayed as white patches. Figure 9 shows that hydrogen diffusion is faster in cases where the shock wave interacts upstream, *i.e.*, when the jet penetration is large. The above observations suggest that the stronger cavity shock at the rear ramp, due to shock wave interaction, causes stronger penetration, resulting in higher mixing efficiency on the upstream side.

The mixing efficiency downstream of the cavity is examined next. As mentioned at the beginning of this section, the mixing efficiency downstream of the cavity increases rapidly when the shock wave impinges on the rear edge of the cavity. To probe into this phenomenon, the distributions of the mass fraction of hydrogen that can be burned and the streamlines are shown in Fig. 10, where, the stoichiometric mass fractions of oxygen and hydrogen are the same as those used in Eq. (1). The mass fractions of burnable hydrogen above 0.016 are shown in color, while those below 0.016 are shown as white patches. Since the hydrogen mass fraction has not exceeded 0.3 in this study, no further colors are defined. The white areas on the mainstream side are due to fuel deficiency, whereas the white areas inside the cavity are due to fuel richness. Figure 10 reveals a difference in the region of fuel richness on the bottom wall downstream of the cavity between the case where the shock wave impinges on the rear edge of the cavity (Case 3) and the other cases. In Case 3, a region of color attaches to the bottom wall at x = 0.07 m, whereas in the other cases, the region of color does not attach to the bottom wall until the location where the reflected shock wave incident occurs (x = 0.07 - 0.09 m). This signifies that in Case 3, the fuel-rich condition near the bottom wall improved upstream to some extent.

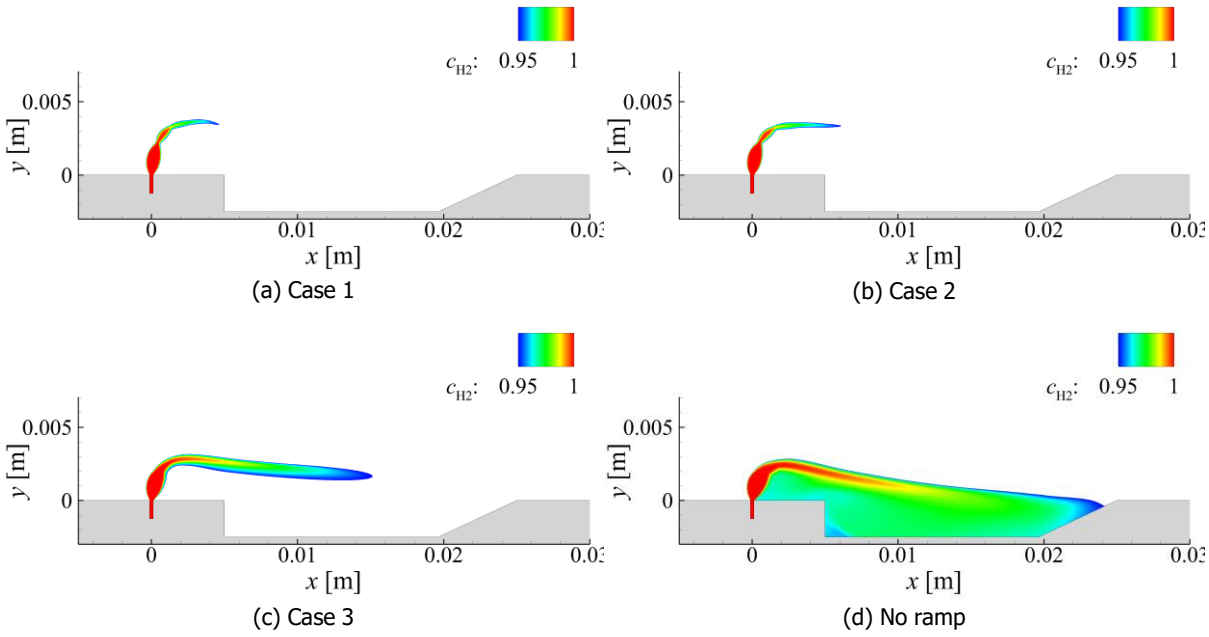

Fig 9. Distributions of regions of high hydrogen mass fraction

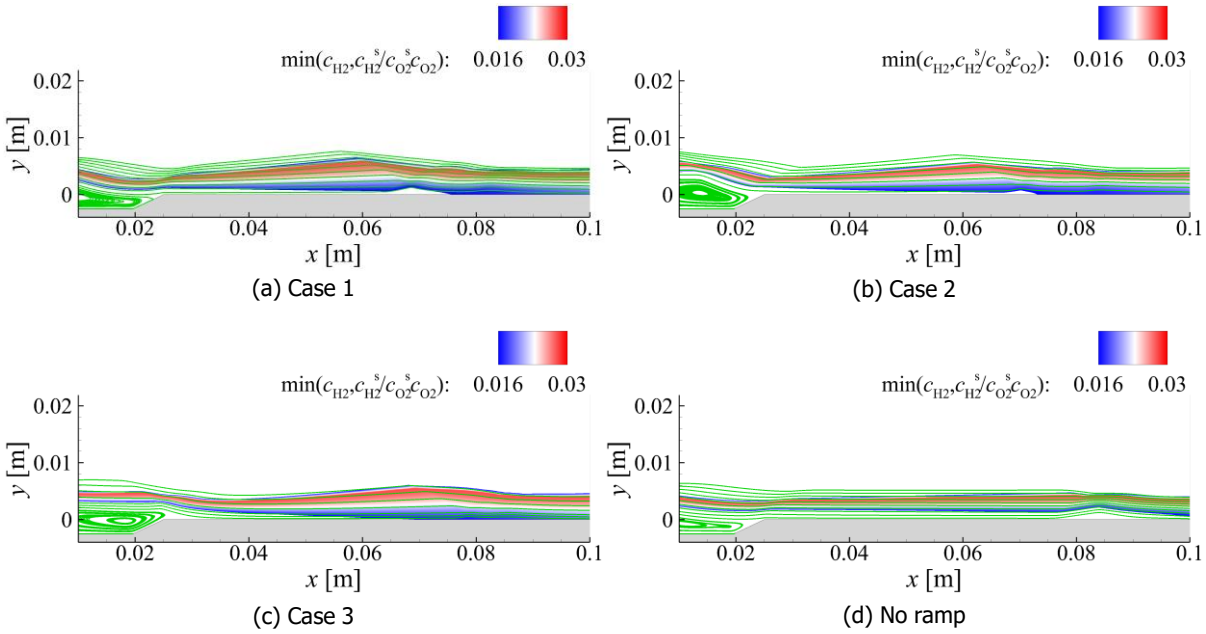

(a) Case 1 (b) Case 2

(c) Case 3 (d) No ramp

Fig 10. Mass fraction distributions and streamline of burnable hydrogen

From the streamlines of Case 3 in Fig. 10, the critical difference between Case 3 and the other cases is the angle of flow at the corner of the cavity rear end. In all cases except Case 3, the flow is in the x-axis direction above the corner. In addition, the main flow is slightly diverted upward by the cavity shock. On the other hand, in Case 3, a recirculation region is formed above the corner, and the mainstream flow toward the wall is formed just downstream of the corner. This is considered to be an oxygen-rich mainstream entering the fuel-rich layer near the wall. The fuel-rich condition at the downstream wall of the cavity has thus been improved, conducing to a rapid increase in the mixing efficiency.

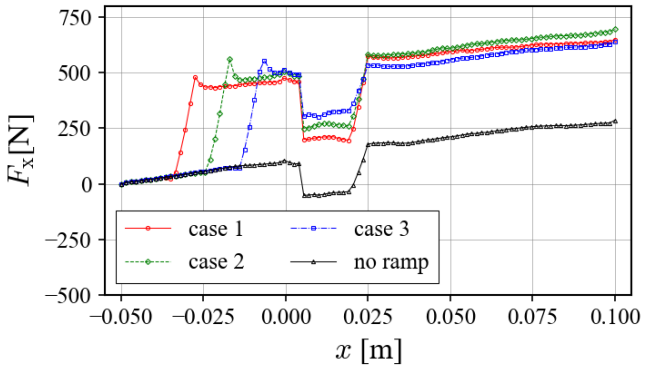

Fig 11. Force variations in streamwise direction

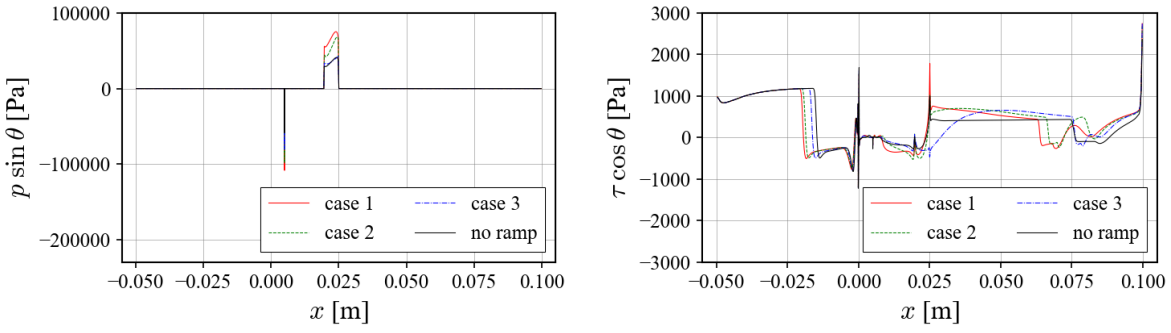

(a) Wall pressure (b) Wall shear stress

Fig 12. Variations of wall pressure and shear stress components in streamwise direction

The variations of the streamwise force among differing shock impingement locations are compared in Fig. 11. The streamwise force is increased by the ramp, decreased by the upstream push on the cavity front wall, and then increased again by the downstream push at the rear ramp. As shown in Fig. 11, the forces on the front and back walls of the cavity increase as the shock impinges upstream. This is due to the higher pressure in the cavity when the shock wave impinges upstream, as observed in Fig. 11. Notably, the forces in the streamwise direction at the rear edge of the cavity (x = 0.025 m) is slightly smaller in Case 3 than in the other cases (Cases 1 and 2). One of the reasons for this is the relatively small pressure increase due to the cavity shock near the cavity ramp, as shown in Fig. 8. To further probe into these observations, Fig. 12 shows the variations of wall pressure and shear stress acting in the streamwise direction. Where the inclination angle θ is positive clockwise with respect to the streamwise direction. The wall pressure distribution shows that the pressure near the cavity ramp in Case 3 is smaller than that in the other cases (Cases 1 and 2), underpinning this discussion. In addition, the wall shear stress distribution shows that the direction in which the acting stress is different from that of the other cases (Cases 1, 2, and no ramp). This is because the rear edge of the cavity is covered by a recirculation region (as shown in Fig. 10), and an upstream flow is formed near the wall. Therefore, it is assumed that the potential strategies to reduce the force in the streamwise direction (drag) in a trapezoidal cavity-based combustor are as follows: 1) suppress the pressure increase due to the cavity shock and 2) completely cover the cavity ramp with the recirculation region.

Conclusions

This study has investigated, the characteristics of fuel mixing due to shock wave interactions in a combustor with transverse injection and cavity-based flameholding with a focus on performance and flowfields. The performance and flowfields have been examined impacting by injecting oblique shock waves at various locations for a specific cavity geometry, and the following findings have been obtained.

The first observation is that the highest mixing efficiency is observed at the combustor outlet when the shock wave impinges on the rear edge of the cavity. This occurs because the mainstream air is diverted towards the wall by the interference of the shock wave and enters the fuel-rich layer near the wall, thus promoting mixing. Secondly, the interaction of the shock wave upstream increases the mixing efficiency around the injector and within the cavity. This is due to the increase in pressure within the cavity, resulting in stronger fuel penetration and enhanced mixing. Thirdly, the lowest drag is observed when the shock wave impinges on the rear edge of the cavity compared to the case with shock wave interaction. This is because the pressure at the cavity ramp depends on the strength of the cavity shock, and because the shear stress acts in the upstream direction due to the recirculation region covering the rear edge of the cavity.

This study has revealed that incident shock waves into a cavity-based combustor can give rise to a variety of flows within the cavity. Since the flow in a cavity also depends on the cavity geometry, it may be possible to produce desirable performance and tailored flowfields by inducing particular shock waves with different cavity geometries.

Acknowledgements

The authors acknowledge the support provided by the Japan Society for the Promotion of Science through JSPS KAKENHI Grant Numbers JP 17K20144 and JPMJSP2136 as well as the Grant-in-Aid for JSPS Fellows Grant Number 22J20613 (22KJ2460).

References

1. Zimont, V., Muhin, E.: Theoretical Maximum Efficiency and Specific Impulse of the External Burning Scramjet. J. Propul. Power (2013). https://doi.org/10.2514/1.B34596
2. Vanyai, T., Bricalli, M., Brieschenk, S., Boyce, R.: Scramjet performance for ideal combustion processes. Aerosp. Sci. Technol. (2018). https://doi.org/10.1016/j.ast.2017.12.021
3. McClinton, C.: X-43 - Scramjet Power Breaks the Hypersonic Barrier: Dryden Lectureship in Research for 2006. AIAA Paper (2006). https://doi.org/10.2514/6.2006-1
4. Smart, M., Hass, N., Paull, A.: Flight Data Analysis of the HyShot 2 Scramjet Flight

Experiment. AIAA J. (2006). https://doi.org/10.2514/1.20661

5. Manna, P., Behera, R., Chakraborty, D.: Liquid-Fueled Strut-Based Scramjet Combustor Design.: A Computational Fluid Dynamics Approach. J. Propul. Power (2008). https://doi.org/10.2514/1.28333
6. Li, L., Huang, Wei., Yan, Li., Du, Z., Fang, M.: Numerical investigation and optimization on the micro-ramp vortex generator within scramjet combustors with the transverse hydrogen jet. Aerosp. Sci. Technol. (2019). https://doi.org/10.1016/j.ast.2018.11.011
7. Freeborn, A., King, P., Gruber, M.: Swept-Leading-Edge Pylon Effects on a Scramjet Pylon-Cavity Flameholder Flowfield. J. Propul. Power (2009). https://doi.org/10.2514/1.39546
8. Lee, S.: Characteristics of Dual Transverse Injection in Scramjet Combustor, Part 1: Mixing. J. Propul. Power (2006). https://doi.org/10.2514/1.14180
9. Fujio, C., Ogawa, H.: Characterization of Shock-Induced Mixing Enhancement for Transverse Injection in Scramjet Engines. AIAA Paper. (2023). https:/doi.org/ 10.2514/6.2023-3053
10. Gruber, M., Baurle, R., Mathur, T., Hsu, K.: Fundamental Studies of Cavity-Based Flameholder Concepts for Supersonic Combustors. J. Propul. Power (2001). https://doi.org/10.2514/2.5720
11. Kim, J., Yoon, Y., Jeung, I., Huh, H., Choi, J.: Numerical Study of Mixing Enhancement by Shock Waves in Model Scramjet Engine. AIAA J. (2003). https://doi.org/ 10.2514/2.2047
12. Mai, T., Sakimitsu, Y., Nakamura, H., Ogami, Y., Kudo, T., Kobayashi, H.: Effect of the incident shock wave interacting with transversal jet flow on the mixing and combustion. Science Direct. (2011). https://doi.org/10.1016/j.proci.2010.07.056
13. Schetz, J., Maddalena, L., Burger, S.: Molecular Weight and Shock-Wave Effects on Transverse Injection in Supersonic Flow. J. Propul. Power (2010). http://dx.doi.org/10.2514/1.49355
14. Ukai, T., Behtash, H., Erdem, E., Lo, K., Kontis, K., Obayashi, S.: Effectiveness of jet location on mixing characteristics inside a cavity in supersonic flow. Exp. Therm. Fluid. Sci. (2014). https://doi.org/10.1016/j.expthermflusci.2013.08.022
15. ANSYS ®Fluent., Release 2023 R1., ANSYS, Inc., Canonsburg, PA, (2022).
16. Geuzaine, C.: Gmsh: A 3-D Finite Element Mesh Generator with Built-in Pre- and Post-Processing Facilities. International Journal for Numerical Methods in Engineering. (2009). https://doi.org/10.1002/nme.
17. Celik, I. B., Ghia, U., Roache, P. J., Freitas, C. J., Coleman, H., Raad, P. E.: Procedure for Estimation and Reporting of Uncertainty Due to Discretization in CFD Applications. J. Fluids. Eng. (2008). https://doi.org/10.1115/1.2960953.